Published in final edited form as:
*Neurobiol Dis*. 2007 May ; 26(2): 481–495. doi:10.1016/j.nbd.2007.02.008.

# Early cerebrovascular and parenchymal events following prenatal exposure to the putative neurotoxin methylazoxymethanol

**Stefania Bassanini**[a,b], **Kerri Hallene**[a], **Giorgio Battaglia**[b], **Adele Finardi**[b], **Stefano Santaguida**[a], **Marilyn Cipolla**[e], and **Damir Janigro**[a,c,d,*]

[a]Department of Cerebrovascular Research, Cleveland, OH, USA

[b]Department of Experimental Neurophysiology, Lab of Molecular Neuroanatomy, Neurological Institute “C. Besta”, Milano, Italy

[c]Department of Cell Biology, The Cleveland Clinic Foundation, Cleveland, OH, USA

[d]Department of Molecular Medicine, Cleveland, OH, USA

[e]The University of Vermont College of Medicine, Burlington, VT, USA

## Abstract

One of the most common causes of neurological disabilities are malformations of cortical development (MCD). A useful animal model of MCD consists of prenatal exposure to methylazoxymethanol (MAM), resulting in a postnatal phenotype characterized by cytological aberrations reminiscent of human MCD. Although postnatal effects of MAM are likely a consequence of prenatal events, little is known on how the developing brain reacts to MAM. General assumption is the effects of prenatally administered MAM are short lived (24 h) and neuroblast-specific. MAM persisted for several days after exposure in utero in both maternal serum and fetal brain, but at levels lower than predicted by a neurotoxic action. MAM levels and time course were consistent with a different mechanism of indirect neuronal toxicity. The most prominent acute effects of MAM were cortical swelling associated with mild cortical disorganization and neurodegeneration occurring in absence of massive neuronal cell death. Delayed or aborted vasculogenesis was demonstrated by MAM's ability to hinder vessel formation. In vitro, MAM reduced synthesis and release of VEGF by endothelial cells. Decreased expression of VEGF, AQP1, and lectin-B was consistent with a vascular target in prenatal brain. The effects of MAM on cerebral blood vessels persisted postnatally, as indicated by capillary hypodensity in heterotopic areas of adult rat brain. In conclusion, these results show that MAM does not act only as a neurotoxin per se, but may additionally cause a short-lived toxic effect secondary to cerebrovascular dysfunction, possibly due to a direct anti-angiogenic effect of MAM itself.

### Keywords

Brain development; Vasculogenesis; Prenatal toxicity; Malformations of cortical development; Angiogenesis; Blood–brain barrier



* Corresponding author. Molecular Medicine, Cleveland Clinic Foundation, NB-20 LRI, 9500 Euclid Ave, Cleveland, OH 44195, USA. Fax: +1 216 445 1466. janigrd@ccf.org (D. Janigro)..

Malformations of cortical development (MCD) are a prominent Dcause of neurological disorders (Battaglia and Basinii, 2006a,b). Prenatal events are a likely cause of human MCD (Ferriero and Dempsey, 1999; Scher, 2003). Common models of MCD consist of prenatal exposure to antiproliferative agents, such as methylazoxymethanol (MAM), and methyl mercury. The proposed mechanism of action leading to MCD is based on toxicity towards differentiating neurons. The corresponding postnatal phenotype will thus be determined by the exact stage of development at which exposure occurs (Bassanini and Battaglia, 2006; Battaglia and Bassanini, 2006a,b; Battaglia et al., 2003a,b).

Methylazoxymethanol is a potent genotoxin, and the aglycone of Cycasin (Balduini et al., 1989; Calcagnotto et al., 2002; Cattabeni and Di Luca, 1997). It is found in the seeds and roots of the Cycad plant (Eizirik and Kisby, 1995; Esclaire et al., 1999). MAM has been used to produce developmental structural abnormalities in the rodent brain (Cattabeni and Di Luca, 1997; Jones and Gardner, 1976). After administration, MAM is converted to methyl-diazonium which is responsible for the methylation of DNA in the O6 and N7 positions of guanine bases (Matsumoto et al., 1972; Nagata and Matsumoto, 1969).

MAM has been proposed to selectively target neuroepithelial cells with an antiproliferative action on dividing, but not quiescent cells (Cattaneo et al., 1995). The antiproliferative effect of this compound has been suggested to occur in a rather narrow time window with a maximal activity at 12 h after administration (Matsumoto et al., 1972). A double dose of MAM administered on gestational day 15 results in a disruption of neuronal cortical layering in the offspring. This is associated with MCD comparable to human periventricular nodular heterotopias (Colacitti et al., 1998; Sancini et al., 1998).

Another example of brain damage after exposure to agents with antimitotic properties is methylmercury fetal poisoning (Battaglia and Bassanini, 2006a,b; Ferriero and Dempsey, 1999). For both models, MAM and methylmercury, orthodoxy cites a neurotoxic mechanism, but several lines of evidence obtained from exposed human or animal brain suggested other cell types. Thus, methylmercury's toxicity was explained by a direct effect on the blood–brain barrier or astrocytes (Bertossi et al., 2004; Qu et al., 2003; Shanker et al., 2003). Similarly, while the commonly accepted mechanism of action of MAM implicates death of vulnerable neuronal precursors, other reports have emphasized vascular changes. A pathological course and marked variability in radial vessel density were seen in cortical areas where neuroblast migration was severely affected (Bardosi et al., 1985a,b, 1987).

Supporting the notion that prenatal vasculogenesis/postnatal angiogenesis may parallel neurogenesis, is the finding that adult neurogenesis is accompanied by the formation of new capillary networks (Haigh et al., 2003; Palmer et al., 2000). Furthermore, the vasculogenesis and angiogenesis inhibitor thalidomide (Franks et al., 2004) causes cortical malformations in humans and animal models (Miyazaki et al., 2005; Narita et al., 2002; Teitelbaum, 2003). We tested the hypothesis that altered vasculogenesis may be an initiator of altered neurogenesis in MAM affected fetal brain.

## Methods

### Animal care and MAM administration

Rats were housed in a controlled environment (21 ± 1 °C; humidity 60%; lights on 08:00 AM–8:00 PM; food and water available ad libitum). Procedures involving animals and their care were conducted in conformity with the institutional guidelines that are in compliance with international laws and policies (EEC Council Directive 86/609, OJ L 358, 1, Dec. 12, 1987; Guide for the Care and Use of Laboratory Animals, U.S. National Research Council, 1996). Pregnant Sprague–Dawley rats received either one or two MAM intraperitoneal (IP)

doses (15 mg/kg of maternal body weight/injection, in sterile saline) on E15 (please note that single injection experiments were used only to compare changes in cell number, see Fig. 3A: CTR or MAM E15/12, and also Fig. 4 Western blot for TUJ-1, E15 and E15/12); in the remainder of the experiments, a double injection was used; the second dose was injected 12 h after the first one. On the same day, control pregnant rats were sham injected with vehicle alone. The day after conception (as determined by vaginal smear) was designated embryonic day 1 (E1). Litter size for MAM-treatment varied between 10 and 13 pups and did not differ significantly from controls.

## Chemicals and reagents

Methylazoxymethanol acetate was purchased from The National Cancer Institute (Bethesda, MD). HPLC grade acetonitrile was purchased from Merck (Darmstadt, Germany). HPLC grade ethanol was purchased from Sigma Aldrich (St. Louis, MO). Milli-Q water (Millipore, Bedford, MA,) was used throughout. The other chemicals used were of analytical reagent grade. Esterase from porcine liver was purchased from Sigma Aldrich (St. Louis, MO).

## HPLC analysis

The chromatographic analysis was carried out according to methods previously described (Fiala et al., 1976). The HPLC system was an Agilent 1100 s HPLC (Agilent, USA) consisting of a quaternary pump and a DAD (Diode Array Detector) set at a wavelength of 217 nm. The analytical column was a micro-bondapak C18 3.9*300 mm from Waters (Milford, MA, USA). The system was run on isocratic gradient utilizing a mobile phase of 1% ethanol in water (v/v) with a run time of 25 min. The chromatographic analysis was performed at room temperature with a flow-rate of 1.0 ml/min and injection volume of 5 μl. Data collection and integration were performed by Agilent Chemstation Software. 100 μl of each serum sample was added to 275 μl of acetonitrile and 20 μl of 0.1 M perchloric acid. The samples were agitated on a vortex mixer and centrifuged for 10 min at 4700×g at 10 °C. The supernatant was collected and filtered in 0.22 um filter unit from Millipore (Carrigtwohill, Ireland) and an aliquot of 5 μl of the filtrate injected into the column for analysis. Brain samples of 0.05–0.5 g were weighed. Sample sizes of 0.1 g were homogenized using a potter in freshly prepared homogenization solution consisting of 0.5 mg/ml of EDTA and 0.5 mg/ml of ascorbic acid in PBS at 4 °C. After complete homogenization, the tissue was added to 675 μl of acetonitrile and 40 μl of 0.1 M perchloric acid; the sample were then agitated on a vortex mixer and centrifuged for 10 min at 4700×g at 10 °C. The supernatant was collected and filtered in 0.22 μm filter unit from Millipore (Carrigtwohill, Ireland) and an aliquot of 5 μl of the filtrate was injected into the column for analysis. Working solutions (10 nM–10 mM) of Methylazoxymethanol acetate were prepared by diluting stock solutions with DMSO. All working solutions were freshly prepared. MAM was prepared by the enzymatic hydrolysis of MAMOAc using porcine liver esterase in potassium phosphate buffer (pH 7.4) at 37 °C for 45 min as previously described (Fiala et al., 1976). The calibration curves for MAM and MAMOAc covered a concentration range of 10 nM −10 mM, constructed by plotting the peak area ratio of the analyte vs. the concentration spiked. Calibration curves were used to obtain the linearity and an independent calibration curve was constructed during each run of experiment. The equations were calculated using linear regression. Concentrations in unknown samples were obtained from the resulting peak area ratios and the regression equation of the calibration curve using back calculation. The limit of quantification for MAM and MAMOAc in both tissue types was 10 nM when an aliquot of 20 μl was injected into HPLC.

## Morphology and densitometry

Animals were perfused at the age of interest with 4% paraformaldehyde in phosphate buffer saline (PB). Brains were subsequently removed, fixed for 2 h in 4% paraformaldehyde, and

cryoprotected in 30% sucrose. One series of cryosectioned brain slices was stained with 1% Cresyl violet or 0.1% thionine for cytoarchitectural analysis; the adjacent sections were processed for immunohistochemistry. Cresyl violet staining was performed on 10–20 μm thick sections. Densitometric analysis was performed using Image Pro Plus 5.0 (Media Cybernetics, Inc.) on representative slices of control and MAM-treated rats. To detect degenerating neuron populations, Fluoro-Jade staining was used (Fernandes et al., 2004). Mounted sections were dried, and placed in 100% ethanol for 3 min followed by 70% ethanol for 1 min. Sections were then placed in water for 1 min, and subsequently placed in 0.06% $KMnO_4$ for 15 min on a shaker. After this, sections were rinsed in water for 1 min and incubated in 0.001% Fluoro-Jade for 30 min on a shaker. Slides were washed in water (3× for 3 min each), dried and mounted with DPX mounting medium. Rat brain sections were also stained with lectin-B to analyze densities and profiles of cerebral blood vessels. Sections were blocked in PBS (1% BSA and 0.5% Triton-X 100) for 1 h at room temperature. They were rinsed in PBS, washed twice with PBLec (PBS, pH 6.8, containing in mM: 0.1 $CaCl_2$, 0.1 $MgCl_2$, 0.1 $MnCl_2$, and 1% Triton-X 100), and incubated in biotinylated isolectin B4 (*Bandeiraea simplicifolia*, Sigma L-2140), 20 μg/ml in PBLec at room temperature for 2 h. After 5 washes with PBS, sections were incubated with Streptavidin conjugates (CY3, Sigma, St. Louis, MO), diluted 1:100 in PBS containing 0.5% BSA and 0.25% Triton-X 100 at room temperature for 2 h. Sections were then rinsed with PBS and coverslipped with Vectashield mounting medium containing DAPI (Vector Laboratories, Burlingame, CA).

To visualize cell nuclei, Vectashield mounting medium with DAPI was used. Immunostaining was performed as previously described (Marroni et al., 2003a,b). Neurotrace™ was used in double-labeling immunofluorescence experiments to visualize neuronal cell bodies. Primary antibodies used were: rabbit anti-aquaporin 1 polyclonal antibody as a marker against a water channel protein expressed in the endothelial cells of blood vessels (1:500; Chemicon International, Temecula, CA), mouse anti-aquaporin 4 monoclonal antibody (1:500; AbCam, Cambridge, MA) as a marker of a water channel protein which is mainly expressed in astroglial end-foot processes, rabbit anti-VEGF, polyclonal antibody against the vascular endothelial growth factor (1:200; Santa Cruz Biotechnologies, Inc, Santa Cruz, CA), anti-Microtubule-Associated Protein-2 (MAP2) SMI-52 (1:500; Sternberger Monoclonals Inc., Lutherville, MA) as a marker of the neuronal cytoskeleton, and guinea pig anti-Doublecortin (DCX) polyclonal antibody that recognize a protein expressed by early migrating neurons (1:3000; Chemicon International, Temecula, CA). Secondary antibodies used were as follows: Texas-red dye conjugated Affinipure donkey anti-mouse IgG (1:1000; Jackson Immunoresearch, West Grove, PA), FITC-conjugated Affinipure donkey anti-rabbit IgG (1:1000; Jackson Immunoresearch, FITC-conjugated Affinipure donkey anti-mouse IgG (1:1000; Jackson Immunoresearch), Texas-red dye conjugated Affinipure donkey anti-guinea Pig IgG (1:1000; Jackson Immunoresearch, West Grove, PA), and Alexa Fluor$^R$ 546 GAM (Molecular Probes diluted 1:2000).

The sections for immunofluorescence were examined on a Leica Aristoplan LS or Radiance 2100 BioRad confocal microscope.

## Angiogenesis experiments

Rat microvascular endothelial cells were cultured as previously described (Marroni et al., 2003a,b; Stanness et al., 1997). Cells were maintained in a humidified 5% $CO_2$ incubator at 37 °C in DMEM (BioWhittaker, Walkersville, MD) with 10% FBS (Sigma, St. Louis, MO) supplemented with 100 U/ml penicillin G, 100 U/ml streptomycin (Gibco BRL, Gaithersburg, MD). Cultures were grown for 2 to 3 days following drug administration and were then examined for signs of toxicity. Cell counts were performed as described (Cucullo

et al., 2005) and data from at least 6 wells per concentration were pooled together. Data are presented as mean±SEM and statistical analysis was performed by ANOVA (Origin V6, Microcal Software, Inc., Northampton, MA). For experiments with Matrigel, cells were first pre-treated for 2 days by culturing on tissue culture dishes. When at 40–60% confluence, cells were released with trypsin/EDTA, washed, spun down, and re-suspended in medium. Matrigel (0.20 mg/ml; BD Bioscience, Bedford, MA) preparation was added at 0.2 ml/$cm^2$ to 48-well plates (Fisher, Pittsburgh, PA); plates were incubated for 30 min at 37 °C in a 5% $CO_2$ humidified chamber; cells were transferred to Matrigel-coated wells and plated at a density of 30,000 cells/$cm^2$. Following 8 h of cell adherence, MAM was added directly to culture media. Cultures were grown for 2 days and the anti-angiogenic effects of the drug were examined. Estimation of tube formation was performed by analyzing images with QCapture Pro Software (Media Cybernetics, San Diego, CA).

### Matrigel in vivo angiogenesis assay and Hemoglobin content

Matrigel (0.20 mg/ml; BD Bioscience, Bedford, MA) matrix and supplies were kept on ice; a wide subcutaneous pocket was formed by swaying the needle right and left after a routine subcutaneous injection. Following this, 500 μl of Matrigel alone or Matrigel+MAM (100 μM) was mixed on ice and subsequently injected into mice subcutaneously with a 21G1 needle. After 3 days of incubation, the mice were anesthetized and ~5 mm square tissue segments containing subcutaneous tissue, peritoneum, and skin were excised with scissors to ensure complete removal of the Matrigel plug. The levels of hemoglobin were analyzed using the Drabkin's Reagent method following the manufacturer's protocol (Sigma, St. Louis, MO).

### DNA fragmentation

DNA fragmentation was measured by gel electrophoresis. DNA was isolated from brain samples using the TRIzol method and following the manufacturer's protocol (Invitrogen, CA). DNA samples were electrophoretically separated on 1% agarose gel containing ethidium bromide (0.5 μg/ml). DNA was visualized by a UV transilluminator and the gels photographed.

### Western blotting

Brains from control and MAM-treated prenatal animals were removed, snap frozen in liquid nitrogen, and stored at −80 °C until use. Protein extracts from control and MAM-treated prenatal rat brains were dissolved in RIPA buffer (radioimmunoprecipitation assay buffer; 0.5% deoxycholic acid, 1% NP-40, 0.1% SDS) containing protease inhibitors (0.17 mg/ml PMSF, 2 μg/ml leupeptin, and 0.7 μg/ml aprotinin; Sigma). Prior to electrophoresis, protein extracts were denatured by heating at 100 °C for 5 min in a running buffer solution containing RIPA, β-mercaptoethanol, and bromophenol blue tracking dye. The acrylamide gel (12%, pre-cast gels; Biorad Labs, Hercules, CA) was run for 2.5–3 h at constant voltage (80 V) until the bromophenol blue tracking dye migrated to the bottom edge of the gel. Proteins from each gel were transferred onto a blot of PVDF membrane using a 192 mM glycine, 25 mM Tris-base, 20% methanol buffer system at constant current (40 mA) overnight at 4 °C. Primary antibodies were: Mouse anti-Beta Tubulin Class III Clone TUJ-1 monoclonal primary antibody (TUJ-1; 1:1000; Chemicon International, Temecula, CA), Mouse anti-aquaporin 4 monoclonal antibody (AQP4; 1:600; abcam, Cambridge, MA), and Anti-Actin (Ab-1) Mouse mAb (JLA20; 1:10000; Calbiochem, Boston, MA). All primary antibodies were probed overnight at 4 °C. Blots were washed and treated with the following secondary antibody: rabbit anti-mouse IgG HRP-conjugated secondary antibody (1:5000; Dako Corporation). Protein concentration was estimated according to the Bradford assay method. Relative expressions of protein were determined by densitometric analysis using Phoretix 1D Advanced Software (Newcastle upon Tyne, UK).

### ELISA

Endothelial cells were seeded (~80,000/$cm^2$) in tissue culture well plates and grown to 90% confluence. Once 90% confluent, MAM (50 μM) was added to the wells. Cells remained in culture with MAM for 48 h; media and the protein were collected from each well (3 wells per treatment: control or MAM). Protein extracts from control or MAM-treated endothelial cells were dissolved in RIPA buffer (radioimmunoprecipitation assay buffer; 0.5% deoxycholic acid, 1% NP-40, 0.1% SDS) containing protease inhibitors (0.17 mg/ml PMSF, 2 μg/ml leupeptin, and 0.7 μg/ml aprotinin; Sigma). Samples were (3 samples/treatment) prepared with appropriate diluent. The protocol was performed according to the manufacturer's details (R and D Systems Human VEGF ELISA, Minneapolis, MN, pp. 6–8).

## Results

For the experiments described here, we used a total of 71 rat pups born from 6 control and 5 MAM-treated dams. Morphological analysis was performed on 22 fetuses (11 controls; 11 MAM); HPLC data were obtained from 35 fetuses (19 controls; 16 MAM); DNA data were obtained from 5 fetuses (3 controls; 2 MAM), and protein data were obtained from 9 fetuses (5 controls; 4 MAM). MAM treatments consisted of either one or two injections performed at E15 at 12 h intervals, as shown in Fig. 1 and in the Methods.

### Pharmacokinetic profile of MAM distribution in the fetal and maternal tissues

We first determined the pharmacokinetic properties of methylazoxymethanol acetate and methylazoxymethanol in maternal serum and fetal brain and liver. MAM-acetate (MAMOAc) was rapidly transformed into MAM and it became undetectable in maternal serum after each injection (↓1 and ↓2 in Fig. 1A). MAM levels grew steadily in the first day of treatment, i.e., 12 and 24 h after the injections, and then slowly declined (Fig. 1A). MAM kinetic profiles and half-lives (around 30 h) in maternal serum were similar to those determined in fetal brain and liver, where virtually identical MAM levels were found (Figs. 1A–C). These results demonstrate a rapid conversion of the injected MAMOAc into MAM, and a longer than expected half-life of the latter, active compound (Colacitti et al., 1999;Matsumoto et al., 1972). In addition, MAM fetal levels were on average 20–25% lower than maternal serum levels, thus suggesting good, but not complete trans-placental distribution and no preferential CNS distribution.

### MAM-induced pathophysiological changes

Since microcephaly is one of the most evident postnatal features of MAM-treated animals (Balduini et al., 1986; Colacitti et al., 1999), we investigated differences in gross anatomical appearance and cortical thickness between MAM-treated and control animals at different developmental stages (Fig. 2). A hypoplastic posterior cortex overlying the superior and inferior collicula, a well known characteristic in MAM animals, was already present at E17 (Fig. 2A) and persisted at later embryonic ages (E19 and E21, not shown). However, the thickness of the developing cortex was increased in MAM animals at E17 and reduced at E19 and E21 when compared to control rats (Fig. 2D). The increase in cortical thickness at E17 was due to a significant enlargement in the size of the extracellular space, as seen in Cresyl violet sections, rather than an increased number of cells (Figs. 2B and C). This was demonstrated by computer-aided quantification of light scatter through comparable coronal brain sections. By this method, the transverse aspect of the cortex (i.e., perpendicular to the pial surface) was digitized and color-coded to reflect the optical density. The procedure was repeated in adjacent and controlateral regions and the data were pooled together. As shown in Fig. 2C1, the dramatic increase in light scatter in cortices from E17 MAM-treated rats reflects an increased size of the extracellular space.

## Prenatal MAM exposure and cell survival

One of the putative mechanisms of action of methylazoxymethanol is direct cellular toxicity resulting in cell death and subsequent reorganization of the cortex and underlying structures (Bassanini and Battaglia, 2006, Battaglia et al., 2003a,b). We attempted to define the time course of these events at early time-points, i.e., 12 h and 24 h after the first MAM treatment (E15/12 and E15/24; Figs. 3A–B), and at E17, E19, and E21 embryonic day (Figs. 3 and 4).

First, cryostat sections were stained with the fluorescent nuclear marker DAPI to obtain reliable cell counting fields. At E17, the density of nuclei in the developing cortex was not significantly different in MAM-treated vs. control animals (Fig. 3E2). In contrast, MAM-induced nuclear shrinkage became apparent 24 h after the first treatment (Fig. 3B), and was markedly evident and statistically significant at E17 (Figs. 3C and E1–E3). At E21, the cortices from MAM-treated and control rats were similar in terms of both cell number and nuclear size (Fig. 3D). We also measured the presence of cell death by different independent methods. By means of Fluoro-Jade staining, a pronounced band of degenerating neurons was present in MAM-treated but not in control cortices at E17 (Fig. 4A). Interestingly, the pattern of Fluoro-Jade staining followed a rostro-caudal gradient of increasing intensity (not shown), similar to the rostro-caudal gradient of cerebral abnormalities observed in adult MAM-treated rats (Colacitti et al., 1999). No degenerating neurons were stained by Fluoro-Jade in control or MAM-treated cortices at E19 (Fig. 4B).

Analysis of genomic DNA laddering revealed no nucleic acid fragmentation (Fig. 4C) and caspase-3 staining was negative (not shown), thus arguing against significant apoptotic changes in E15 to E19 MAM-treated cortices. Finally, western blot analysis with an anti-TUJ-1 antibody, a marker of neuronal precursor cells (Heidmets et al., 2006), revealed no evident reductions of TUJ-1 levels in MAM-treated vs. control rats at all time-points tested (E15/12 to E21, Fig. 4D). Taken together, these data suggest that direct, MAM-induced neuronal degeneration was not a predominant feature of the effects of MAM, or at least confined to a narrow time-window, and presumably not related to apoptotic pathways. However, the possibility that necrotic cell death occurs, cannot be entirely ruled out.

## MAM and neuronal differentiation

Prenatal neuronal effects of MAM are obvious candidates for postnatal brain development abnormalities. Therefore, we studied the effects of MAM by using neuronal differentiation markers at a time when cortical development reaches its maximal growth and when edema induced by MAM may affect neuronal maturation or migration. To this end, sections were processed with antibodies against Doublecortin (DCX), a cytoskeletal protein expressed early by migrating neuroblasts and antibodies against the neuronal marker MAP2 (Figs. 5A and B). While there was an obvious difference between MAM and naive cortex at days E17, these differences were less pronounced when one took into account the marked swelling and edema of MAM cortex (Fig. 5C1). Densitometric analysis and tracing of DCX and MAP2 immunopositive cells and cellular processes demonstrated that the MAM cortex was characterized by a qualitative but not quantitative difference in immunostaining (Fig. 5C2), since a comparable number of cells were stained in both MAM and naive brain. However, the staining pattern with both antibodies in both the cortical plate and the subcortical areas was markedly irregular, particularly in the subventricular zone. In particular, the orientation of cells was clearly disorganized when compared to naive cortex. These results indicate that MAM, although not exerting significant cell lethality, was nevertheless able to disrupt cell migration at developmental stages as early as E17, which resulted in significant cytoarchitectural abnormalities.

### Prenatal MAM and vasculogenesis

Previous reports (Bardosi et al., 1985a,b; Bardosi et al., 1987; Hallene et al., 2005) suggested that in addition to parenchymal toxicity, methylazoxymethanol may also affect, directly or indirectly, vasculogenesis. Similar conclusions were recently reached in a Thalidomide model of cortical malformation (Hallene et al., submitted for publication). To further investigate the possibility of MAM acting on vasculogenesis, we processed cortical sections with immunological markers of the cerebral vasculature (Fig. 6). VEGF immunoreactivity clearly outlined vascular profiles in naive animals (Fig. 6A). Both penetrating and superficial pial vessels were stained. In contrast, E17 MAM cortices were virtually devoid of VEGF staining (right panel in Fig. 6A). We also investigated the pattern of expression of isolectin B4, an endothelial marker, and aquaporin1, an endothelial water channel marker. Both experiments revealed a significantly reduced vascular density in cortices from MAM-treated rats (Figs. 6C and D). In the case of AQP1, a western blot analysis for AQP4 was performed to assess the specificity of the effects (see inset in D). In addition, we wished to confirm that VEGF was one of the main targets of MAM. This was performed by measuring intracellular (synthesis) and extracellular (release) VEGF in endothelial cell cultures exposed to MAM (see ELISA). Note that MAM (75 μM) caused a pronounced and statistically significant reduction of both VEGF pools.

Based on these morphological data in vivo and the reduced expression of VEGF in vitro after exposure to MAM, we performed various in vitro and in vivo experiments to asses the potency of MAM in inhibiting endothelial cell differentiation (Akhtar et al., 2002). The results shown in Fig. 7A demonstrate that in vitro angiogenesis of rat brain microvascular endothelial cells is inhibited at micromolar concentrations of methylazoxymethanol; at the same concentrations, MAM failed to induce a significant toxicity as indicated by cell counts shown in Fig. 7B. Note that endothelial MAM toxicity and cell death were only seen at concentrations well in excess of 100 μM. In vivo assays were performed in mice bearing MAM- or saline-soaked Matrigel plugs (Akhtar et al., 2002)(Fig. 7C). Note that MAM (100 μM) decreased vessel formation as estimated by measurements of hemoglobin content after 3 days. These results demonstrate that one of the effects of prenatal exposure to MAM is reduced cortical vasculogenesis, possibly due to a direct action on vessel formation.

Since MAM-treated brains were characterized by altered cortical vasculogenesis, we further investigated the anatomy of penetrating pial vessels in brains of MAM-treated compared to non-treated rats (Fig. 8). In contrast to the normal “radial” appearance of cortical vessels in E19 control rats (Figs. 8A–A1), in MAM animals, cortical vessels were large, abnormally branched, and in close association with clusters of heterotopic neurons, i.e., groups of neurons that appeared misplaced compared to normal cortex (Figs. 8B–B1). In addition, apparently dead-ending vessels, or vessels not tapering after branching, or returning toward the pial surface, were also observed (Figs. 8C–C1).

Similar vascular abnormalities were also found in early postnatal stages (Fig. 9). At these developmental stages, the strict anatomical relation between abnormal vessels and clusters of abnormally positioned neurons became more evident. In particular, columnar clusters of heterotopic cells were frequently observed, surrounding very large and abnormally branched vessels. This feature was clearly evident in thionine-stained sections (Figs. 9A and B), as well as in sections double-labeled with neuronal and vascular markers (Fig. 9C). The confocal immunofluorescence analysis of these cellular clusters demonstrated that the vast majority of these cells revealed a neuronal phenotype (Fig. 9C). These results, taken together with published reports by others (Abe et al., 1997;Barkovich et al., 1992;Fernandez-Bouzas et al., 2006;Hodozuka et al., 2000;Jay et al., 1993;Kakita et al., 2002;Kuchna et al., 1995;Landrieu and Lacroix, 1994;Striano et al., 2000), show that there is a concomitant and typographically localized development of vascular abnormalities and

cell migration defects/abnormal heterotopic clustering in both human dysplastic and MAM-treated cortex.

There is an obvious alternative explanation for our results, which are MAM-mediated toxic effects on neuronal parenchyma affecting vascular development. Our experiments were not designed to address this important temporal sequence of events, but our results are rather to support the hypothesis that MAM's action affects both vascular and neuronal development to eventually produce the cerebral malformations observed in the postnatal brain. Finally, we have verified whether the observed abnormalities of penetrating pial vessels were associated also with vascular alterations at the capillary level. This is an important issue since neural vascular coupling is most crucial at the microvascular level. In postnatal MAM-treated rats (around 30 days postnatal), the capillary density surrounding abnormal, large penetrating pial vessels was clearly lower than in control animals (Fig. 10A). By contrast, cortical regions where abnormal pial penetrating vessels were not present had normal capillary density as compared to control (Fig. 10B). Thus, the microscopic maldevelopment of penetrating pial vessels is associated with a hypo-density of capillary networks in the cortical regions of MAM-treated animals characterized by clusters of heterotopic neurons. This defect was circumscribed to the region surrounding abnormal arteries, but was absent in other regions, which were presumably fed by normal vasculature.

## Discussion

We analyzed with a combination of different techniques, early cellular events following the administration of MAM, a compound used to induce experimental developmental MCD. The main finding is that the putative neurotoxin MAM does not appear to cause postnatal neuronal abnormalities exclusively based on a cytotoxic action. Furthermore, we have demonstrated that in addition to parenchymal cells, MAM has a powerful effect on the development of the cerebrovasculature. This is supported by experimental findings including (1) intrauterine MAM brain levels after single and double injections never reached values that cause cell death (Battaglia et al., 2003a,b; Cattabeni and Di Luca, 1997; Cattaneo et al., 1995); (2) at low concentrations, as those that were persistent after injection of pregnant rats, MAM affected (and partially aborted) vasculogenesis and angiogenesis both in vitro and in vivo; and (3) a number of measurements of neuronal viability, differentiation, and migration demonstrated that MAM exerted only a modest acute effect on these cells.

MAM has been used to study the effects of early ablation of neurons on postnatal cortical development. It was hypothesized that neuronal loss at a crucial prenatal stage causes abnormalities in developed brain (Battaglia et al., 2003a,b). The mechanism proposed was based on MAM's capacity to cause a selective, time-restricted toxicity against early differentiating neuroepithelium (Cattaneo et al., 1995; Colacitti et al., 1999). It was assumed that MAM distributes to the fetal brain at concentrations sufficient to cause neuronal death during a timeframe restricted to the short half-life of the toxin (Battaglia et al., 2003a,b). The present experiments demonstrate a more complex mechanism of action, indicating that MAM may act not only on neuroblasts, but also directly on the cerebrovasculature.

Our first novel finding is that intrauterine brain levels after MAM E15 injections never reached values shown to determine cell death, about 750 μM (Battaglia et al., 2003a,b; Cattabeni and Di Luca, 1997; Cattaneo et al., 1995). We show that MAM does not preferentially accumulate, but distributes equally from maternal serum to the fetal brain, reaching levels in the low micro-molar range, well below frankly cytotoxic levels. Note that the studies cited before used “normal” culture conditions, while our data suggest that inhibited vasculogenesis may have caused hypoxia/hypoglycemia, both potentially acting as “sensitizing agents” favoring the ill effects of MAM on cell survival.

In addition, contrary to what is commonly assumed, MAM half-life is clearly longer than that reported in previous literature (for example see Cattaneo et al., 1995). Therefore, MAM is likely to exert a prolonged action on neuroblast proliferation (Cattaneo et al., 1995) or neuroblast survival (Esclaire et al., 1999), presumably between E15 and E17. In this time period, the existence of MAM-induced neuronal damage is supported by the presence of cortical swelling due to cytotoxic edema, the positive staining for FluoroJade, and the significant reduction of the nuclear size within the cortex observed at E17. In addition, MAM-related altered patterns of neuronal migration were demonstrated by the clear irregularity of doublecortin and MAP2 staining in the developing cortical plate and subventricular zone from E17 onwards. The absence of DNA laddering and caspase-3 staining also supports the fact that MAM treatment does not trigger functionally relevant apoptotic mechanisms of cell death, even if the presence of MAM-induced necrotic neuronal damage cannot be ruled out.

We explored other mechanisms including a possible action on differentiating or newly formed blood vessels. Blood supply to the brain is a crucial aspect of CNS physiology, and altered cerebral blood flow or other forms of vascular defects are the most common cause of neurological disorders. It was therefore possible that MAM may exert a direct effect on vascular cells or cells responsible for vascular development. Our results in vitro and in vivo (Figs. 7A–C) clearly show that at concentrations consistent with the low end of those observed after prenatal exposure, MAM can effectively decrease vasculogenesis without causing significant cellular death. It was only at higher concentrations that loss of an angiogenic response was due to direct cell death. This was shown for rat brain endothelial cells *in vitro*, and by a Matrigel plug assay model *in vivo*. The relevance of an anti-angiogenetic effect exerted by MAM in our experimental condition is also underscored by the fact that in early postnatal as well as adult MAM-treated brain the heterotopic clusters of neurons are always associated with abnormal vessels, either penetrating pial vessels or vessels in the underlying white matter. Such vessels not only show a preferential anatomical localization within the heterotopic structures, but they are also characterized by abnormal features, in terms of size, absence of tapering off after vascular ramification, and presence of irregular branches abnormally returning vs. the pial surface.

If one of the targets of MAM is the developing blood vessel, how may the neuronal defects, observed postnatally, be explained by this new mode of action? Our data clearly suggest that MAM treatment deeply affects the neurovascular unit of the developing brain. While it is possible, and so-far accepted, that MAM-induced effects on the neural parenchyma may determine vascular abnormalities, our data also suggest that abnormal vascular development may in turn cause abnormal neuronal migration patterns. This concept is supported by the fact that the prenatal administration of thalidomide, a known and selective angiogenesis inhibitor, may induce cerebral malformations sharing similarities with those observed in MAM-treated rats (Hallene et al., submitted for publication). The observed signs of neuronal damage may be in part related to transient deprivation of oxygen and nutrients, perhaps combined with the low clearance of metabolites as one would expect to occur following decreased vasculogenesis in a rapidly growing cortex. Therefore, the proposed sequence of events may be as follows (Fig. 11). Injection of MAM does not directly affect in a toxic way any vascular cells, but rather inhibits proliferation of cells required to build new vessels for a rather prolonged period of time. During the same timeframe, MAM also impairs the proliferation of neuroepithelial cells (Cattaneo et al., 1995; Battaglia et al., 2003a,b) and modestly alters neuroblast survival (Esclaire et al., 1999). Both effects may be aggravated by concomitant reduction in metabolic supply. These events, combined, alter the migration of subsequent waves of young neurons (Battaglia et al., 2003a,b). The rapid growth of the cortex at E15–19 is therefore transiently stunted by a combined affect of decreased vasculogenesis, impaired neurogenesis, and cytotoxic and subdural edema. When the effects

of MAM wane, the vasculature can reposition itself in the cortex, neurogenesis recovers, and both edema and subdural enlargement disappear. However, this combination of events deeply alters the normal development of the neurovascular structure, and clusters of newly formed neuronal cells still populate the regions of the abnormal blood vessels.

Our results extend several observations and conclusions drawn previously (e.g. Battaglia et al., 2003a,b; Flagstad et al., 2005; Flagstad et al., 2004; Lavin et al., 2005; Lu et al., 2000). Even if several reports, including the majority of those addressing the altered neuronal excitability (Calcagnotto et al., 2002, Calcagnotto and Baraban, 2003; Castro et al., 2002) in MAM animals, have used a single injection approach with higher MAM doses, presumably leading to lower and less persistent levels of the toxic period, our data apply to both procedures of MAM treatment. Furthermore, studies support our conclusions, including those demonstrating a clear-cut interdependence of the cerebrovasculature with neuronal malformations and adult neurogenesis (Bardosi et al., 1985a,b; Bardosi et al., 1987; Palmer et al., 2000).

Several questions remain unanswered. First, how does MAM affects vascular development? MAM is fundamentally a chemotherapic agent, and these agents are known to affect both rapidly proliferating cells and endothelium (Mailloux et al., 2001). Furthermore, it is not clear how the MAM-induced vascular defect and the related transient hypo-perfusion of the cortex may contribute to abnormal clustering of neurons. A parsimonious explanation of this fact is that migrating neurons may be attracted by oxygen and glucose gradients thus tending to cluster in regions where the vascular supply is still present. Whether misplaced neurons might use the vascular system as guide to migrate within the subcortical and cortical regions needs to be explored further. However, the data presented here underscore the possibility that vascular dysgenesis is one of the mechanisms leading to malformation of cortical development.

## References

Abe T, Singer RJ, Marks MP, Kojima K, Watanabe M, Uchida M, Hayabuchi N. Arterial vascular abnormality accompanying cerebral cortical dysplasia. AJNR Am. J. Neuroradiol 1997;18:144–146. [PubMed: 9010533]

Akhtar N, Dickerson EB, Auerbach R. The sponge/Matrigel angiogenesis assay. Angiogenesis 2002;5:75–80. [PubMed: 12549862]

Balduini W, Cimino M, Lombardelli G, Abbracchio MP, Peruzzi G, Cecchini T, Gazzanelli GC, Cattabeni F. Microencephalic rats as a model for cognitive disorders. Clin. Neuropharmacol 1986;9(Suppl. 3):S8–S18. [PubMed: 3594461]

Balduini W, Lombardelli G, Peruzzi G, Cattabeni F, Elsner J. Nocturnal hyperactivity induced by prenatal methylazoxymethanol administration as measured in a computerized residential maze. Neurotoxicol. Teratol 1989;11:339–343. [PubMed: 2796888]

Bardosi A, Ambach G, Friede RL. The angiogenesis of micrencephalic rat brains caused by methylazoxymethanol acetate: II. Superficial and basal arterial system. Acta Neuropathol. (Berl) 1985a;68:59–64. [PubMed: 4050354]

Bardosi A, Ambach G, Friede RL. The angiogenesis of micrencephalic rat brains caused by methylazoxymethanol acetate: I. Superficial venous system. A quantitative analysis. Acta Neuropathol. (Berl) 1985b;66:253–263. [PubMed: 4013676]

Bardosi A, Ambach G, Hann P. The angiogenesis of the micrencephalic rat brains caused by methylazoxymethanol acetate: III. Internal angioarchitecture of cortex. Acta Neuropathol. (Berl) 1987;75:85–91. [PubMed: 3434219]

Barkovich AJ, Gressens P, Evrard P. Formation, maturation, and disorders of brain neocortex. AJNR Am. J. Neuroradiol 1992;13:423–446. [PubMed: 1566709]

Bassanini, S.; Battaglia, G. Cell Cycle in the Nervous System. Janigro, D., editor. Humana Press; 2006.

Battaglia, G.; Bassanini, S. Cell Cycle in the Nervous System. Janigro, D., editor. Humana Press; 2006a. p. 43-55.

Battaglia, G.; Bassanini, S. Models of Seizures and Epilepsy. Pitkanen, A.; Schwartzkroin, PA.; Moshe, SL., editors. Elsevier; Burlington, MA: 2006b. p. 305-314.

Battaglia G, Bassanini S, Granata T, Setola V, Giavazzi A, Pagliardini S. The genesis of epileptogenic cerebral heterotopia: clues from experimental models. Epileptic Disord 2003a;5(Suppl. 2):S51–S58. [PubMed: 14617421]

Battaglia G, Pagliardini S, Saglietti L, Cattabeni F, Di Luca M, Bassanini S, Setola V. Neurogenesis in cerebral heterotopia induced in rats by prenatal methylazoxymethanol treatment. Cereb. Cortex 2003b;13:736–748. [PubMed: 12816889]

Bertossi M, Girolamo F, Errede M, Virgintino D, Elia G, Ambrosi L, Roncali L. Effects of methylmercury on the microvasculature of the developing brain. Neurotoxicology 2004;25:849–857. [PubMed: 15288515]

Calcagnotto ME, Baraban SC. An examination of calcium current function on heterotopic neurons in hippocampal slices from rats exposed to methylazoxymethanol. Epilepsia 2003;44:315–321. [PubMed: 12614386]

Calcagnotto ME, Paredes MF, Baraban SC. Heterotopic neurons with altered inhibitory synaptic function in an animal model of malformation-associated epilepsy. J. Neurosci 2002;22:7596–7605. [PubMed: 12196583]

Castro PA, Pleasure SJ, Baraban SC. Hippocampal heterotopia with molecular and electrophysiological properties of neocortical neurons. Neuroscience 2002;114:961–972. [PubMed: 12379251]

Cattabeni F, Di Luca M. Developmental models of brain dysfunctions induced by targeted cellular ablations with methylazoxymethanol. Physiol. Rev 1997;77:199–215. [PubMed: 9016302]

Cattaneo E, Reinach B, Caputi A, Cattabeni F, Di Luca M. Selective in vitro blockade of neuroepithelial cells proliferation by methylazoxymethanol, a molecule capable of inducing long lasting functional impairments. J. Neurosci. Res 1995;41:640–647. [PubMed: 7563244]

Cavaglia M, Dombrowski SM, Drazba J, Vasanji A, Bokesch PM, Janigro D. Regional variation in brain capillary density and vascular response to ischemia. Brain Res 2001;910:81–93. [PubMed: 11489257]

Colacitti C, Sancini G, Franceschetti S, Cattabeni F, Avanzini G, Spreafico R, Di Luca M, Battaglia G. Altered connections between neocortical and heterotopic areas in methylazoxymethanol-treated rat. Epilepsy Res 1998;32:49–62. [PubMed: 9761308]

Colacitti C, Sancini G, De Biasi S, Franceschetti S, Caputi A, Frassoni C, Cattabeni F, Avanzini G, Spreafico R, Di Luca M, Battaglia G. Prenatal methylazoxymethanol treatment in rats produces brain abnormalities with morphological similarities to human developmental brain dysgeneses. J. Neuropathol. Exp. Neurol 1999;58:92–106. [PubMed: 10068317]

Cucullo L, Dini G, Hallene KL, Fazio V, Ilkanich EV, Igboechi C, Kight KM, Agarwal MK, Garrity-Moses M, Janigro D. Very low intensity alternating current decreases cell proliferation. Glia 2005;51:65–72. [PubMed: 15779084]

Eizirik DL, Kisby GE. Cycad toxin-induced damage of rodent and human pancreatic beta-cells. Biochem. Pharmacol 1995;50:355–365. [PubMed: 7646537]

Esclaire F, Kisby G, Spencer P, Milne J, Lesort M, Hugon J. The Guam cycad toxin methylazoxymethanol damages neuronal DNA and modulates tau mRNA expression and excitotoxicity. Exp. Neurol 1999;155:11–21. [PubMed: 9918700]

Fernandes AM, Maurer-Morelli CV, Campos CB, Mello ML, Castilho RF, Langone F. Fluoro-Jade, but not Fluoro-Jade B, stains non-degenerating cells in brain and retina of embryonic and neonatal rats. Brain Res 2004;1029:24–33. [PubMed: 15533312]

Fernandez-Bouzas A, Harmony T, Santiago-Rodriguez E, RicardoGarcell J, Fernandez T, Avila-Acosta D. Schizencephaly with occlusion or absence of middle cerebral artery. Neuroradiology 2006;48:171–175. [PubMed: 16391916]

Ferriero DM, Dempsey DA. Impact of addictive and harmful substances on fetal brain development. Curr. Opin. Neurol 1999;12:161–166. [PubMed: 10226748]

Fiala ES, Bobotas G, Kulakis C, Weisburger JH. Separation of 1,2-dimethylhydrazine metabolites by high-pressure liquid chromatography. J. Chromatogr 1976;117:181–185. [PubMed: 1249149]

Flagstad P, Mork A, Glenthoj BY, van Beek J, Michael-Titus AT, Didriksen M. Disruption of neurogenesis on gestational day 17 in the rat causes behavioral changes relevant to positive and negative schizophrenia symptoms and alters amphetamine-induced dopamine release in nucleus accumbens. Neuropsychopharmacology 2004;29:2052–2064. [PubMed: 15199377]

Flagstad P, Glenthoj BY, Didriksen M. Cognitive deficits caused by late gestational disruption of neurogenesis in rats: a preclinical model of schizophrenia. Neuropsychopharmacology 2005;30:250–260. [PubMed: 15578007]

Franks ME, Macpherson GR, Figg WD. Thalidomide. Lancet 2004;363:1802–1811. [PubMed: 15172781]

Haigh JJ, Morelli PI, Gerhardt H, Haigh K, Tsien J, Damert A, Miquerol L, Muhlner U, Klein R, Ferrara N, Wagner EF, Betsholtz C, Nagy A. Cortical and retinal defects caused by dosage-dependent reductions in VEGF-A paracrine signaling. Dev. Biol 2003;262:225–241. [PubMed: 14550787]

Hallene K, Oby E, Marchi N, Janigro D. Impaired vasculogenesis as a mechanism of CNS malformation. Epilepsia 2005;46:8.

Hallene K, Oby E, Lee BI, Santaguida S, Bassanini S, Cipolla M, Marchi N, Hossain M, Battaglia G, Janigro D. Pre-natal exposure to Thalidomide, altered vasculogenesis, and central nervous system malformations. submitted for publication.

Heidmets LT, Zharkovsky T, Jurgenson M, Jaako-Movits K, Zharkovsky A. Early post-natal, low-level lead exposure increases the number of PSA-NCAM expressing cells in the dentate gyrus of adult rat hippocampus. Neurotoxicology 2006;27:39–43. [PubMed: 16169083]

Hodozuka A, Hashizume K, Nakai H, Tanaka T. Vascular abnormalities in surgical specimens obtained from the resected focus of intractable epilepsy. Brain Tumor Pathol 2000;17:121–131. [PubMed: 11310919]

Jay V, Becker LE, Otsubo H, Hwang P, Hoffman HJ, Armstrong DC. Neuronal heterotopia with capillary penetration of neurons and cortical dysplasia in a patient with complex partial seizures. Case report. J. Neurosurg 1993;78:654–657. [PubMed: 8450340]

Jones MZ, Gardner E. Pathogenesis of methylazoxymethanol-induced lesions in the postnatal mouse cerebellum. J. Neuropathol. Exp. Neurol 1976;35:413–444. [PubMed: 932788]

Kakita A, Hayashi S, Moro F, Guerrini R, Ozawa T, Ono K, Kameyama S, Walsh CA, Takahashi H. Bilateral periventricular nodular heterotopia due to filamin 1 gene mutation: widespread glomeruloid microvascular anomaly and dysplastic cytoarchitecture in the cerebral cortex. Acta Neuropathol. (Berl) 2002;104:649–657. [PubMed: 12410386]

Kisby GE, Kabel H, Hugon J, Spencer P. Damage and repair of nerve cell DNA in toxic stress. Drug Metab. Rev 1999;31:589–618. [PubMed: 10461542]

Kisby GE, Standley M, Lu X, O'Malley J, Lin B, Muniz J, Luo NL, Pattee P, Back SA, Nagalla SR. Molecular networks perturbed in a developmental animal model of brain injury. Neurobiol. Dis 2005;19:108–118. [PubMed: 15837566]

Kuchna I, Iwanowski L, Dambska M. Vascular malformations associated with other congenital anomalies of the central nervous system: coexistence and possible causal relations. Folia Neuropathol 1995;33:255–259. [PubMed: 8673436]

Landrieu P, Lacroix C. Schizencephaly, consequence of a developmental vasculopathy? A clinicopathological report. Clin. Neuropathol 1994;13:192–196. [PubMed: 7955664]

Lavin A, Moore HM, Grace AA. Prenatal disruption of neocortical development alters prefrontal cortical neuron responses to dopamine in adult rats. Neuropsychopharmacology. 2005

Lu MH, Tang N, Ali SF. Effects of single injection of methylazoxymethanol at postnatal day one on cell proliferation in different brain regions of male rats. Neurotoxicology 2000;21:1145–1151. [PubMed: 11233761]

Mailloux A, Grenet K, Bruneel A, Beneteau-Burnat B, Vaubourdolle M, Baudin B. Anticancer drugs induce necrosis of human endothelial cells involving both oncosis and apoptosis. Eur. J. Cell Biol 2001;80:442–449. [PubMed: 11484935]

Marroni M, Agarwal M, Kight K, Hallene K, Hossain M, Cucullo L, Signorelli K, Namura S, Janigro D. Relationship between expression of multiple drug resistance proteins and p53 tumor suppressor gene proteins in human brain astrocytes. Neuroscience 2003a;121:605–617. [PubMed: 14568021]

Marroni M, Kight KM, Hossain M, Cucullo L, Desai SY, Janigro D. Dynamic in vitro model of the blood–brain barrier. Gene profiling using cDNA microarray analysis. Methods Mol. Med 2003b; 89:419–434. [PubMed: 12958437]

Matsumoto H, Spatz M, Laqueur GL. Quantitative changes with age in the DNA content of methylazoxymethanol-induced microencephalic rat brain. J. Neurochem 1972;19:297–306. [PubMed: 5010077]

Miyazaki K, Narita N, Narita M. Maternal administration of thalidomide or valproic acid causes abnormal serotonergic neurons in the offspring: implication for pathogenesis of autism. Int. J. Dev. Neurosci 2005;23:287–297. [PubMed: 15749253]

Nagata Y, Matsumoto H. Studies on methylazoxymethanol: methylation of nucleic acids in the fetal rat brain. Proc. Soc. Exp. Biol. Med 1969;132:383–385. [PubMed: 5344864]

Narita N, Kato M, Tazoe M, Miyazaki K, Narita M, Okado N. Increased monoamine concentration in the brain and blood of fetal thalidomide- and valproic acid-exposed rat: putative animal models for autism. Pediatr. Res 2002;52:576–579. [PubMed: 12357053]

Palmer TD, Willhoite AR, Gage FH. Vascular niche for adult hippocampal neurogenesis. J. Comp. Neurol 2000;425:479–494. [PubMed: 10975875]

Qu H, Syversen T, Aschner M, Sonnewald U. Effect of methylmercury on glutamate metabolism in cerebellar astrocytes in culture. Neurochem. Int 2003;43:411–416. [PubMed: 12742086]

Sancini G, Franceschetti S, Battaglia G, Colacitti C, Di Luca M, Spreafico R, Avanzini G. Dysplastic neocortex and subcortical heterotopias in methylazoxymethanol-treated rats: an intracellular study of identified pyramidal neurones. Neurosci. Lett 1998;246:181–185. [PubMed: 9792622]

Scher MS. Prenatal contributions to epilepsy: lessons from the bedside. Epileptic Disord 2003;5:77–91. [PubMed: 12875951]

Shanker G, Syversen T, Aschner M. Astrocyte-mediated methylmercury neurotoxicity. Biol. Trace Elem. Res 2003;95:1–10. [PubMed: 14555794]

Stanness KA, Westrum LE, Fornaciari E, Mascagni P, Nelson JA, Stenglein SG, Myers T, Janigro D. Morphological and functional characterization of an in vitro blood–brain barrier model. Brain Res 1997;771:329–342. [PubMed: 9401753]

Striano S, Nocerino C, Striano P, Boccella P, Meo R, Bilo L, Cirillo S. Venous angiomas and epilepsy. Neurol. Sci 2000;21:151–155. [PubMed: 11076003]

Teitelbaum P. A proposed primate animal model of autism. Eur. Child. Adolesc. Psychiatry 2003;12:48–49. [PubMed: 12601565]

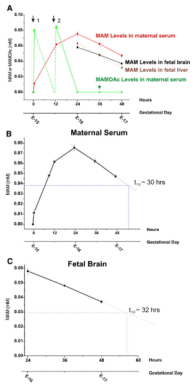


**Fig. 1.**

Pharmacokinetic properties of methylazoxymethanol acetate (MAMOAc) and MAM. (A) Following intraperitoneal injection at E15, MAMOAc (*green line*) was, as expected, rapidly converted into MAM and became undetectable 12 h after each injection (indicated by ↓1 and ↓2). After each injection, MAM levels detected in maternal serum steadily increased for about 12 h. The half value of the rising time was on average 7.7 h. MAM levels then declined over the following several days. The kinetic properties of MAM found in maternal serum were similar to those observed in fetal brain and liver, suggesting that MAM was not preferentially distributed into the CNS. (B, C) The measured half-lives in maternal serum and fetal brain were virtually identical (approximately 32 h). Data are presented as mean ± SEM.

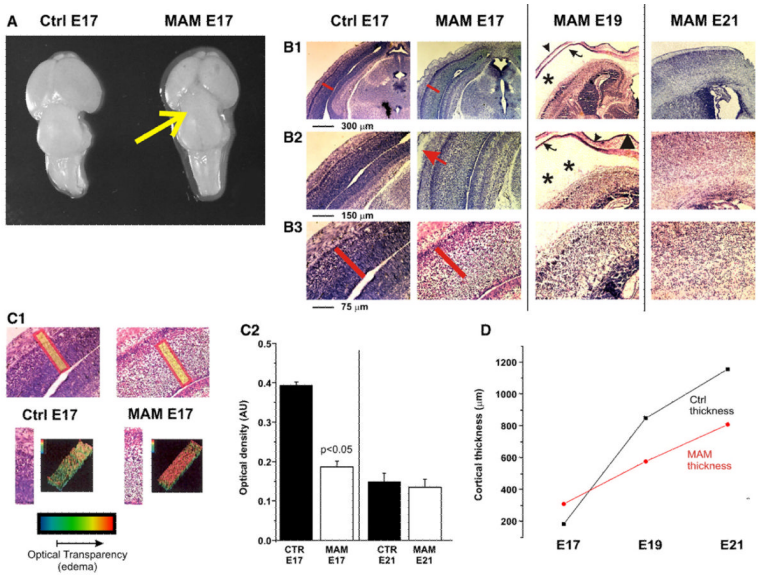


**Fig. 2.**

MAM-induced effects on cortical size and histology. (A) Gross anatomy: as early as 48 h after first MAM exposure, an evident shrinkage of the posterior cortex covering the superior and inferior collicula (*yellow arrow*), a common characteristic of adult MAM-treated brains, was clearly present. Scale bar: 1 mm. (B) Cresyl violet staining was used to examine the effects of MAM on cortical organization at different time-points (E17 to E21). A remarkable increase in cortical thickness was the first significant difference observed in the cortices of E17 MAM-treated rats compared to control. The *red bars* in B1 and B2 have identical length to show the increased thickness of the cortex at E17 in MAM or control brain. Cortical thickness was reduced at later time-points if compared to controls. Another feature of MAM-treated cortices was the apparent increase in subdural space. Subdural external hydrocephalus was already apparent at E17 (*red arrow* in B2), and peaked at E19 (*asterisks* in B1, B2). (C) Computer-aided analysis examining optical density demonstrates that cortical thickening at E17 was not a consequence of increased cell number, but rather due to an increase in the extracellular space. Note the dramatic increase in light scatter in MAM cortices (C1), indicative of an enhanced size of the acellular matrix. Histograms in C2 quantify this finding at E17 ($n$=4; $p$<0.05), and demonstrate no differences in extracellular space at E21 between MAM-treated and control rats. (D) Comparison between cortical thicknesses in MAM-treated vs. controls at different time-points. Note the transient initial cortical swelling in MAM fetuses (E17), and the consistently reduced thickness of MAM-treated rats if compared to controls. (For interpretation of the references to colour in this figure legend, the reader is referred to the web version of this article.)

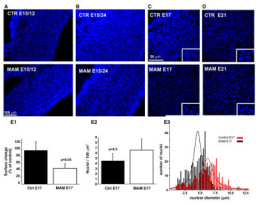

**Fig. 3.**

Cell death after MAM treatment. (A–D) Comparison between MAM treated and control cortices stained with the fluorescent marker DAPI at different time-points. Twelve hours after the first injection (A, E15/12), DAPI staining revealed neither obvious changes in cell number nor chromatin condensation. However, 24 h after the first MAM treatment (B, E15/24), nuclear shrinkage and chromatin aggregation became apparent. This effect was overly prominent at E17 (C, compare higher magnification inserts), but was barely visible at E21 (D). (E) Quantification of MAM effects on nuclear condensation and cell numbers, as determined by DAPI staining. Note the significant decrease in nuclear size induced by MAM (E1; $p<0.05$; $n=3$), by contrast the total number of cells (determined by measurements of nuclear density) was not significantly different when compared to control (E2). The histogram in E3 illustrates the dramatic nuclear shrinkage induced by MAM at E17.

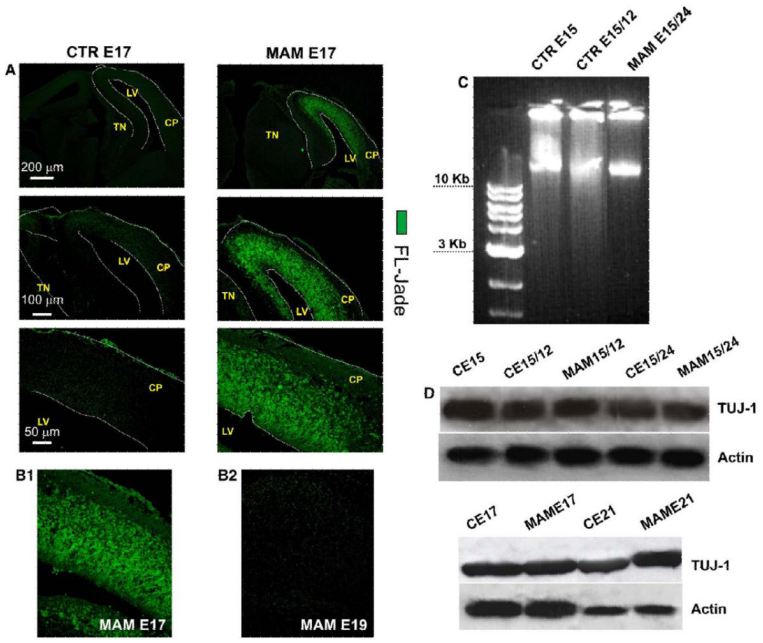


**Fig. 4.**

Neuronal degeneration is confined to a restricted time window after MAM exposure. (A) Fluoro-Jade (FJ) staining was performed on sections adjacent to those stained with Cresyl violet and DAPI (see Figs. 2 and 3; CP=cortical plate, Tn=Thalamic nuclei, LV=lateral ventricle). FJ staining consistently revealed a pronounced band of degenerating neurons in MAM E17 cortex, whereas no FJ positive neurons were found in naive animals (A). At E19, no FJ-stained neurons were evident in either MAM-treated or control brains (compare B1 and B2), thus suggesting that MAM-induced neuronal degeneration was temporally segregated. (C) Analysis of genomic DNA revealed no nucleic acid fragmentation (DNA laddering), suggesting that apoptotic changes were not a prominent effect of MAM treatment. (D) Western blotting with the TUJ-1 antibody, a marker of newly differentiated neurons, revealed similar protein levels in both treated and untreated cortices at all time-points tested, indicating that neuronal cell loss was not a major effect of MAM treatment. Note the evident decrease of TUJ-1 expression levels between E15 and E21, likely due to the maturation of neurons. The *lower* band refers to probing with antibodies against actin, used as control for protein loading.

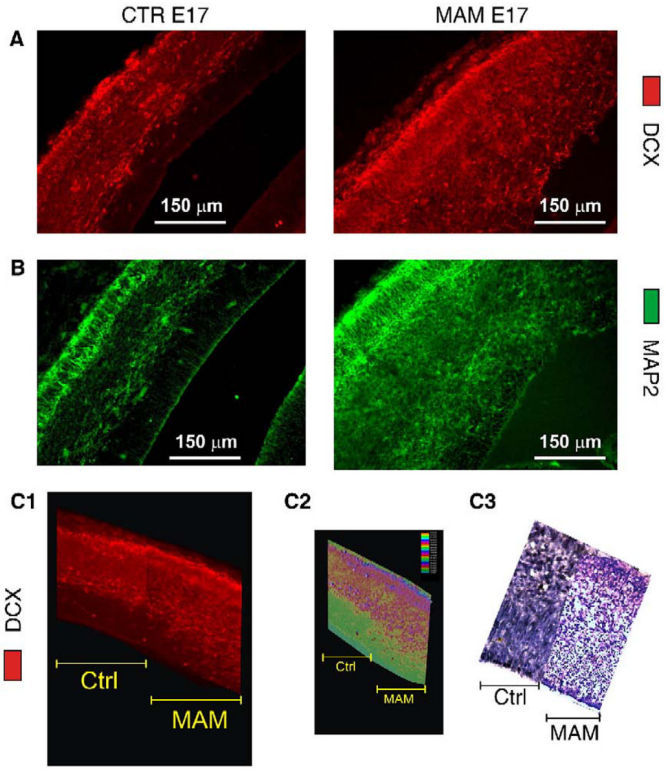


**Fig. 5.**

Prenatal brain development and cytoarchitectural abnormalities. (A, B) Coronal brain sections from E17 cortex were processed with antibodies anti-doublecortin (DCX; in red), a marker of early migrating neurons, and anti-MAP-2 (green), an early marker of differentiated neurons. Note the cortical disorganization of MAM-treated rats when compared to naive animals, and the staining with both antibodies of the sub-ventricular zone close to the ventricle. The cortical disorganization in MAM rats was less obvious when two cortical sections were normalized by their size (C1), suggesting that edema also contributed to DCX/MAP-2 distribution changes; the irregular staining of the sub-ventricular zone remained, however, a prominent feature of the MAM-treated cortex. (C2) Tracing and densitometric analysis of MAP-2 and DCX positive cells and cell processes revealed qualitative but not quantitative differences in MAM cortex. A neighboring set of sections (C3) were stained with Cresyl violet to demonstrate the level of extracellular space enlargement in MAM cortex.

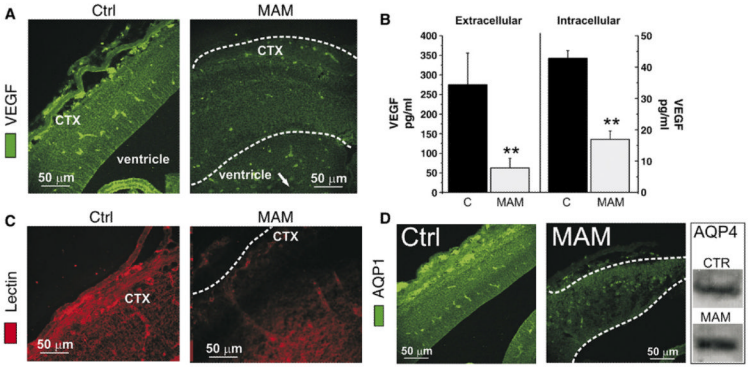


**Fig. 6.**

MAM-induced abnormalities of blood vessels in vivo. (A, C, D) Immunostaining with VEGF (A), isolectin B4 (C), and AQP1 (D) antibodies was used to visualize vascular and endothelial elements in MAM-treated animals and controls. VEGF, isolectin, and AQP1 staining revealed visibly outlined vascular profiles in control animals (*left panels* in A, C, and D). In contrast, there was a considerable decrease in vascular staining in cortices from MAM-treated rats (*right panels* in A, C, and D). The specificity of the effect was tested in the case of AQP1 by Western analysis of AQP4, which was virtually unchanged (see western bands in the *right panel* of D). The effects on VEGF were confirmed by ELISA (B): note the decreased levels of VEGF in endothelial cells grown for 3 days after confluence in the presence or absence of 50 μM MAM. The *asterisks* indicate $p<0.02$. The effects of MAM were evident when analyzing both intracellular and secreted protein levels.

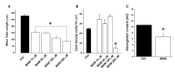

**Fig. 7.**

MAM-induced abnormalities of angiogenesis in vitro and in vivo. (A) Matrigel angiogenesis assay. Note that all concentrations (10–200 μM) of MAM dramatically reduced Matrigel-induced tube formation in endothelial cells exposed to the drug for 2 days. All MAM data points were statistically significant when compared to control ($p<0.05$; $n=6$ wells per concentration) with the exception of 10–100 μM in the cell density assay. (B) In vitro drug toxicity studies: parallel experiments were also performed on fibronectin-coated plates to test for lethality/toxicity induced by MAM. Concentrations of MAM (0–200 μM) while capable of inhibiting angiogenesis, did not cause appreciable toxicity to cells. Note that cell death only occurred when the highest concentration of MAM was used (200 μM). (C) In vivo Matrigel plug assay: the assay was performed to test the ability of MAM (100 μM) in the inhibition of angiogenesis. Matrigel plugs inserted into mice resulted in large capillary networks as demonstrated by measurements of hemoglobin levels in the resected tissue. Note that MAM caused a statistically significant ($p<0.05$, $n=5$) decrease in plug vascularization.

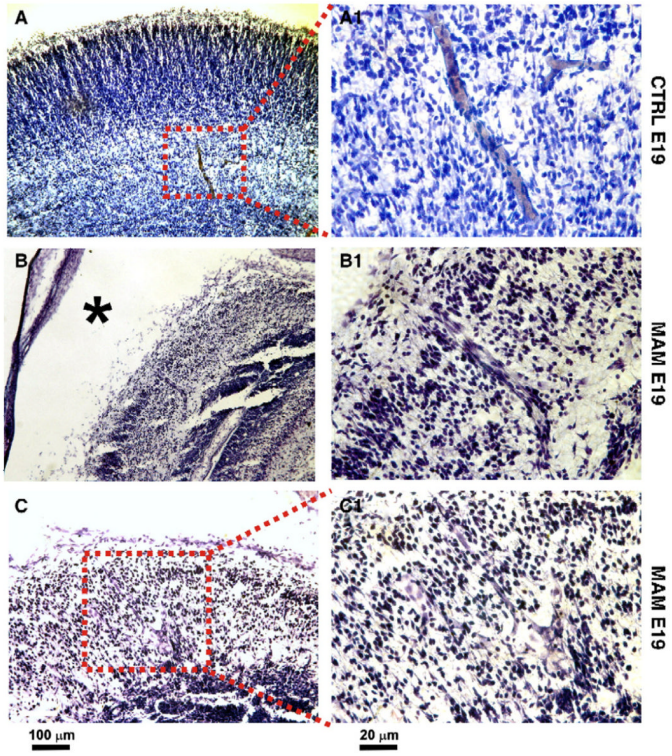


**Fig. 8.**

Abnormal vascular development in prenatal MAM brain (E19). Note that normal appearing vessels (A, A1) were not surrounded by any significant clustering of cellular elements compared to MAM (B, B1). Also note the large sub-dural space indicated by an asterisk (B). The abnormality at the vascular level was also evident when analyzing patterns of branching pial vessels (C). Observe that MAM-treated cortex was filled with vessels that did not become significantly smaller in size after branching, nor did the branching vessels penetrate deeper in cortex, but rather sometimes returned toward the pial level as shown in the enlargement in C1. The outlined drawings in *red* show vascular shape as traced from the micrographs. Sections were stained with thionine. (For interpretation of the references to colour in this figure legend, the reader is referred to the web version of this article.)

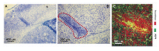

**Fig. 9.**

Abnormal neurovascular clustering in early postnatal MAM cortex. (A–B) Note the clustering of parenchymal cells surrounding pial vessels in MAM-treated animals (P7). (C) The neuronal origin of the majority of the cells surrounding the vessels was demonstrated by double labeling experiments with Neurotrace™ (*red*, to emphasize neurons) and the glial endfoot marker AQP4 (*green*) analyzed by confocal microscopy.

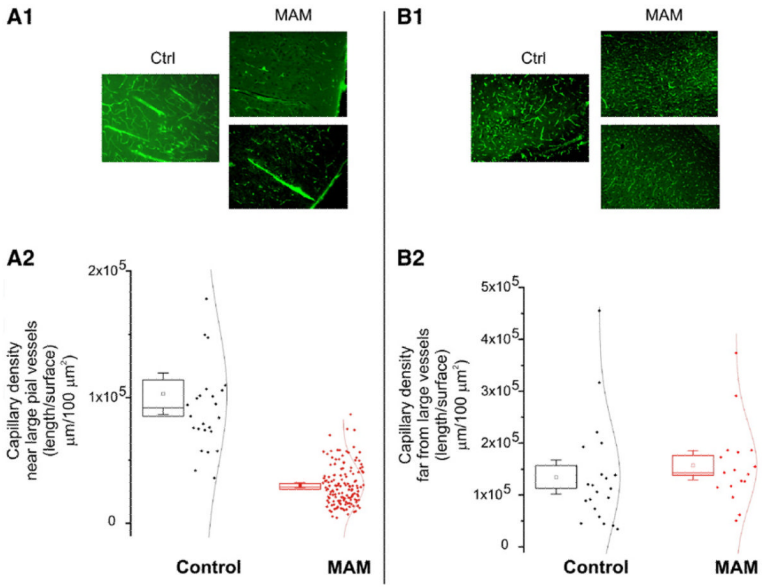


**Fig. 10.**

Persistence of microvascular changes in adult MAM rats. Capillary density was quantified as described elsewhere (Cavaglia et al., 2001). Note that in proximity to large primitive appearing vessels in MAM animals (left panel) the capillary density was significantly lower than in comparable regions in control animals (A1, A2). In contrast, regions distal to penetrating pial vessels were endowed by comparable capillary density in MAM and naive animals (B1, B2).

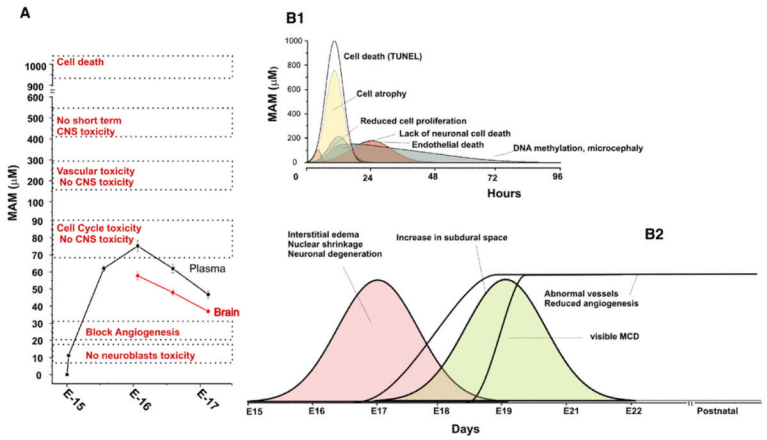


**Fig. 11.**

Summary and interpretation of the results. See text and discussion for full explanation. (A) Relationship between measured MAM levels and MAM's concentrations needed to exert various effects. The measured brain and serum levels of MAM are well below the concentrations needed to exert direct neurotoxicity in vitro (Cattaneo et al., 1995; Esclaire et al., 1999; Kisby et al., 1999, 2005; Matsumoto et al., 1972), or direct endothelial cell toxicity (our results, Fig. 6). At the concentrations measured in our experiments, the conceivable mechanisms of action of MAM include reduced vasculogenesis, impaired proliferation of neuroepithelial cells, and perhaps a modest effect on neuroblast survival. (B1) Summary of experimental evidences (Cattaneo et al., 1995; Esclaire et al., 1999; Kisby et al., 1999; 2005; Matsumoto et al., 1972), used to support a neurotoxic, neuron-specific and temporally defined action of MAM. Emphasis is put on the temporal profile and MAM levels necessary to achieve any given effect. Compare the quantitative and temporal profiles with the measured MAM levels depicted in A. (B2) Experimental evidence presented here implicates possible alternative explanations of MAM's action. Cerebral edema, external hydrocephalus, and decreased vasculogenesis are early hallmarks of MAM's action.